biblio.ugent.be

The UGent Institutional Repository is the electronic archiving and dissemination platform for all UGent research publications. Ghent University has implemented a mandate stipulating that all academic publications of UGent researchers should be deposited and archived in this repository. Except for items where current copyright restrictions apply, these papers are available in Open Access.

This item is the archived peer-reviewed author-version of: The effect of nanoparticle degradation on poly(methacrylic acid)-coated quantum dot toxicity: the importance of particle functionality assessment in toxicology

Authors: Soenen S.J., Montenegro J-M., Abdelmonem A.M., Manshian B.B., Doak S.H., Parak W.J., De Smedt S.C., Braeckmans K.

In: Acta Biomaterialia, 10(2), 732-741 (2014)

Optional: link to the article

To refer to or to cite this work, please use the citation to the published version:

Authors (year). Title. *journal Volume(Issue)* page-page. Doi 10.1016/j.actbio.2013.09.041

The effect of nanoparticle degradation on poly(methacrylic acid)-coated quantum dot toxicity: the importance of particle functionality assessment in toxicology.

Stefaan J. Soenen[a,b], José-Maria Montenegro[c], Abuelmagd M. Abdelmonem[c], Bella B. Manshian[d], Shareen H. Doak[d], Wolfgang J. Parak[c,e], Stefaan C. De Smedt[*,a], and Kevin Braeckmans[a,b]

[a] Faculty of Pharmaceutical Sciences, Ghent University, Ghent, Belgium.

[b] Center of Nano- and Biophotonics, Ghent University, Ghent, Belgium.

[c] Department of Physics, Philipps University of Marburg, Marburg, Germany

[d] DNA Damage Group, Swansea University, Swansea, UK.

[e] CIC biomaGUNE, San Sebastián, Spain

Corresponding author: Fax: +32 9264 8189

Tel: +32 9264 8076

E-mail: Stefaan.Desmedt@ugent.be

Abstract

Colloidal semiconductor nanoparticles (quantum dots) have attracted a lot of interest in technological and biomedical research, given their potent fluorescent properties. However, the use of heavy metal-containing nanoparticles remains an issue of debate. The possible toxic effects of quantum dots remain a hot research topic and several questions such as possible intracellular degradation of quantum dots and the effect thereof on both cell viability and particle functionality remain unresolved. In the present work, poly(methacrylic acid)-coated CdSe/ZnS quantum dots were synthesized and characterized, after which their effects on cultured cells were evaluated using a multiparametric setup. The data reveal that the quantum dots are taken up through endocytosis and when exposed to the low pH of the endosomal structures, they partially degrade and release cadmium ions, which lowers their fluorescence intensity and augments particle toxicity. Using the multiparametric method, the quantum dots were evaluated at non-toxic doses in terms of their ability to visualize labeled cells for longer time periods. The data revealed that comparing different particles in terms of their applied dose is challenging, likely due to difficulties in obtaining accurate nanoparticles concentrations, but evaluating particle toxicity in terms of their biological functionality enables an easy and straightforward comparison.

1. Introduction.

The use of colloidal nanoparticles (NPs) in technological and biomedical applications is vastly increasing [1, 2]. There are currently over 800 consumer products containing NPs including many foods, beverages and cosmetics. The nanotechnology industry is growing very rapidly, predicted to have a total value of $3.1 trillion by the year 2015 [3]. Currently, NPs are omnipresent in many different consumer products, but the number of biomedical applications is still limited due to several questions remaining on the possible induction of toxic side-effects by NPs [4-6]. Uncertainties regarding the safety of NPs are being fed by the continuous discovery of new pathways and mechanisms by which NPs may interfere with cellular wellbeing, which can either be beneficial for biomedical purposes or pose serious threats to human health [7]. One example is the recent finding that NPs can induce DNA damage and chromosome mutations, as shown for carbon nanotubes that were found to selectively stabilize human telomeric i-motif DNA and inhibit telomerase activity [8]. To progress towards use of NPs without risks, more data are required on the (toxic) effects of NPs on cells, tissues and whole organisms [9]. In order to fulfill the current needs in nanotoxicity research, NPs should be screened rapidly on a variety of cells under standardized conditions, enabling a comparison of data obtained for different materials and between different research groups [10]. In this view, we recently established a multiparametric methodology that looks at the interactions between cultured cells and NPs in order to get a profound knowledge of the possible effects of these materials on cultured cells [11]. Using a variety of cell types that have shown great potential for nanotoxicity research [12-14], being primary human umbilical vein endothelial cells (HUVECs), murine C17.2 neural progenitor cells and rat PC12 pheochromocytoma cells, the obtained results are representative for a wide variety of cell types. This methodology therefore allows for determining the non-cytotoxic levels of NPs

(i.e. the concentration of NPs appropriate for cell labeling applications) and additionally helps in unraveling the mechanisms that are involved in the cytotoxic profile of the NPs under investigation. Furthermore, by comparing the data obtained against data for other NPs that have been tested under identical conditions, physicochemical features of the NPs that contribute to their cytotoxicity can be defined, paving the way for a more rational and safer NP design.

One important aspect with respect to rigorous NP toxicity testing is the design, purification and characterization of the NPs under investigation [15]. If any cytotoxic effects are to be ascribed to specific physicochemical features of the NPs, it is of utmost importance to test well-characterized NPs free of contaminants or impurities [16]. In this direction, poly(methacrylic acid) (PMA)-coated CdSe/ZnS core-shell quantum dots (QDots) are a useful system, as these NPs are well defined and have been extensively characterized. QDots are small semiconductor NPs that possess several exciting features such as high photostability, narrow and tunable emission spectra and high brightness [17]. Owing to these properties, QDots have shown great potential for many biomedical applications, including cell labeling applications [18-21], long-term tracking of (single) molecules [22], *in vivo* imaging [23, 24] and photodynamic therapy [25, 26]. However, despite their excellent photophysical properties, their toxicity, in particular due to the release of Cd^{2+} ions [27, 28], remains an issue of debate [29, 30].

2. Materials and Methods.

2.1. Nanoparticles.

CdSe/ZnS colloidal nanoparticles were synthesized and made water-soluble as described in the Supplementary Information. The nanoparticles were carefully characterized as also described in full detail in the accompanying Supplementary Information.

2.2. Cell culture.

C17.2 neural progenitor cells and PC12 cells are maintained in high glucose Dulbecco's Modified Eagle's Medium (DMEM), supplemented with 10% fetal bovine serum, 5% horse serum, 2 mM L-Glutamine and 1% Penicillin/Streptomycin (Gibco, Invitrogen, Merelbeke, Belgium). Cells were maintained in a humidified atmosphere at 5% CO2 and fresh medium was given every other day. C17.2 cells were passaged (1/10) when reaching 90% confluency. PC12 cells were grown in 25 cm² cell culture flasks (Corning, Amsterdam, The Netherlands) that were coated with collagen (rat tail collagen type I, Invitrogen, Belgium) and passaged (1/5) when growing in small clumps (approximately 5 cells/clump and reaching 70-80% confluency). Fresh medium was given every other day.

For some long-term experiments, such as the effect of intracellular pH on Cd^{2+} in time, and the toxicity derived from this free Cd^{2+}, non-proliferating cell cultures are required as dilution of the number of particles per cell due to cell division abolishes any attempt to analyze these parameters. Therefore, in the current study, non-proliferating cell populations were established to enable to investigate the time-dependent effects of the intracellular environment on QDot functionality and toxicity. Next to analyzing these effects without the problem of exponential QDot dilution, these conditions also better mimic the *in vivo* conditions where autologous cells or stem cells after transplantation show minimal proliferation. To establish non-proliferating cell populations, cells were exposed with 60 μM Apigenin (Sigma-Aldrich, Bornem, Belgium) together with the Sil NP exposure. After removal of the medium, fresh media containing 60 μM Apigenin was used, where media were replaced for 50% every other day with fresh Apigenin-containing medium for the duration of the experiments. Under these conditions, cell death was found to be minimal and cell proliferation was reduced to approximately 9% of the normal value.

Furthermore, removal of the medium with normal cell culture medium not containing any Apigenin resulted in a recovery of cell proliferation to near-control levels after approximately three days.

Primary human umbilical vein endothelial cells (HUVECs) were kindly provided by Dr. Aldo Ferrari (ETH Zurich, Switzerland). For cultivation, cells were kept in 75 cm² cell culture flasks (Corning, Amsterdam, The Netherlands) coated with collagen (rat tail collagen type I, Invitrogen, Belgium) prior to cell seeding. The cells were maintained in endothelial cell basal growth medium and growth supplement (Cell Applications, Tebu-Bio, Le Perray en Yvelines, France) and passaged (1/5) when reaching 80-90% confluency. Every other day, fresh medium was given. For HUVEC cells, the Apigenin treatment resulted in slight toxic effects and proliferation could be impeded better using serum-free conditions. To establish non-proliferating HUVEC cultures, cells were given endothelial cell serum-free defined medium (Cell Applications, Tebu-Bio, Le Perray en Yvelines, France) when reaching high levels of confluency. Confluent HUVEC monolayers could then be maintained for at least one week without any observable signs of cell death or ROS induction.

2.3. Cell-nanoparticle interaction studies.

The following cell-NP interactions were studied, where a full methodology can be found in the Supplementary Information that accompanies this manuscript:

2.3.1. Intracellular QDot localization.

To evaluate possible endosomal localization of the QDots, C17.2, HUVEC or PC12 cells were seeded in collagen-coated 35 mm diameter glass bottom MatTek dishes (MatTek Corporation, Ashland, MA, USA) at $4*10^4$ cells/dish in 1.5 mL of full culture medium. Cells were allowed to settle overnight prior to being incubated with the lipophilic membrane tracer dye 3,3′-dioctadecyloxacarbocyanine perchlorate (DiO; Molecular Probes, Invitrogen, Belgium) for 30 min at 2.5 µg/mL. Next, a mixture of the QDot at 15 nM and the lipophilic dye DiO (2.5 µg/mL) in full cell medium was prepared and added to the cells for 30 min at 37 °C at a humidified atmosphere. Subsequently, the media were removed, cells washed three times with PBS and fixated with 4% paraformaldehyde (PFA) for 15 min at ambient temperature prior to visualization using a Nikon Cs1 confocal laser scanning microscope (Nikon Belux, Brussels, Belgium).
Cellular uptake of the PMA-coated QDots was also evaluated using transmission electron microscopy, following 24 h exposure oft he various cell types to 10 nM of QDots, as described in the Supplementary Information.

2.3.2. Quantitative determination of cellular QDot levels.

The number of QDots per cell was determined by measuring the cellular Cd^{2+} levels using the Measure-iT kit (Molecular Probes, Invitrogen, Merelbeke, Belgium) as described in the Supplementary Information.

2.3.3. Effect of pH on QDot stability.

The effect of pH on QDot fluorescence intensity and release of Cd^{2+} ions was determined by preparing 3 buffer solutions of pH 7.4, 5.5 and 4.5, respectively; after which the QDots (5 nM)

were exposed to these buffers for a period up to 5 days. Every 24 h, fluorescence intensity or Cd^{2+} release was measured, as described in the Supplementary Information.

2.3.4. Determination of intracellular QDot degradation.

C17.2, PC12 or HUVEC cells were seeded in 75 cm² cell culture flasks at a density of $2.5*10^6$ cells/flask and allowed to settle overnight. Then, the cells were given fresh medium containing 10 nM of QDots and allowed to incubate for 24 h. For C17.2 and PC12 cells, their medium was supplemented with 60 μM Apigenin. For HUVEC cells, cells were allowed to form confluent monolayers after cell labeling and medium was transferred to serum-free defined medium for culture of non-proliferative HUVECs. Next, media were aspirated, cells washed twice with PBS and fresh media optimized for non-proliferating cultures was given as described above after which the cells were kept in culture for the duration of the experiment. After 1, 2, 3, 4 and 5 days of further culture under proliferation-restricted conditions, cells from the various flasks were lifted and centrifuged at 0.4 rcf. The cells were redispersed in PBS and counted using a Bürker chamber. Then, $2*10^6$ cells were taken, which were centrifuged again after which 50 μL of DMSO was added to every pellet to lyse all cells. A 10 μL aliquot was collected from every sample and transferred to wells of a 96-well plate after which 200 μL/well of the Measure-iT kit was added and Cd^{2+} concentrations were measured according to the manufacturer's instructions (λ_{ex}: 490 nm; λ_{em}: 520 nm) using a Wallac Envision plate reader instrument. The Cd^{2+} concentrations were determined using the Cd^{2+} calibration curve which is part of the kit. Please note that as this is an end-point assay, the samples measured after 1, 2, 3, 4, and 5 days were all

obtained from different flasks. Data are expressed as mean ± SEM for three independent experiments.

Along with the determination of free cellular Cd^{2+} levels, the total Cd^{2+} levels were determined at the same time points as described above. These data revealed no significant differences in the total Cd^{2+} content (both free and QDot-associated) at the different time points. Previous experiments furthermore revealed no interference of the QDots themselves with the assay readout, see Supplementary Information Section V.

For $CdCl_2$-treated cells, a similar approach was followed, where cells were incubated with $CdCl_2$ at different concentrations (0, 1, 5, 20, 50, 100, 250 or 500 nM) for 24 h after which the cells were washed twice with PBS, lifted and centrifuged at 0.4 rcf. The cells were redispersed in PBS and counted using a Bürker chamber. Then, $2*10^6$ cells were taken, which were centrifuged again after which 50 µL of DMSO was added to every pellet to lyse all cells and Cd^{2+} concentrations were then determined as described above.

2.3.5. Determination of cell viability.

Cell viability for all three cell types was assessed using an MTT assay, both in proliferative and in non-proliferative cell populations. This assay was performed both for cells exposed to QDots and cells exposed to $CdCl_2$. A full description of both methodologies can be found in the accompanying Supplementary Information.

2.3.6. Determination of reactive oxygen species.

Induction of reactive oxygen species for all three cell types was assessed using 10 μM 5-(and-6)-chloromethyl-2',7'-dichlorodihydrofluorescein diacetate, acetyl ester (CM-H_2DCFDA; Molecular Probes, Invitrogen, Merelbeke, Belgium), both in proliferative and in non-proliferative cell populations. This assay was performed both for cells exposed to QDots and cells exposed to $CdCl_2$. A full description of both methodologies can be found in the accompanying Supplementary Information.

2.3.7. Determination of mitochondrial membrane potential and DNA damage.

For these studies, cells were incubated with the PMA-coated QDots for 24 h at various concentrations (from 0 to 30 nM) after which mitochondrial membrane potential was evaluated spectrofluorometrically using 20 μM JC-10 dye and DNA damage was assessed by staining for phosphorylated γ-H2Ax using fluorescent antibodies followed by fluorometric plate reading as described in full in the Supplementary Information.

2.3.8. Determination of HUVEC cell morphology.

The morphology of HUVEC cells was evaluated by exposing the cells to the PMA-coated QDots for 24 h at concentrations at which no acute toxicity was noticed (up to 20 nM), after which cells were stained for Tubulin and F-Actin and visualized using a Nikon Cs1 confocal laser scanning microscope as described in the Supplementary Information.

2.3.9. Determination of PC12 functionality.

The ability of PC12 cells to induce neurite sprouting was evaluated after exposing the cells for 24 h to the PMA-coated QDots at concentrations at which no acute toxicity or effects on cell morphology were noticed (up to 10 nM). After QDot-exposure, the cells were incubated with nerve growth factor for 48 h and stained for α-tubulin followed by confocal laser scanning analysis as described in the Supplementary Information.

2.3.10. Determination of QDot transfer in proliferating cells.

QDot distribution in proliferation cells was evaluated as follows: C17.2, PC12 or HUVEC cells were seeded at $1.25*10^5$ cells/flask (5 mL total medium) and allowed to settle overnight after which the cells were incubated with the QDots at 0 or 2 nM for 24 h. Following incubation, media were aspirated, cells washed twice with PBS, lifted by trypsin and kept in culture in full medium, without any QDots, where for half of the dishes, cells were reseeded in MatTek dishes at $2.5*10^4$ cells/dish and $1.25*10^5$ cells/flask every other day either at the odd or even days after QDot exposure. The cells reseeded in the flasks were kept in culture for 2 more days and then treated similarly for the duration of the experiment (a total of 9 days), where the MatTek seeded cells were allowed to settle for 2 h. Prior to analysis, media were removed, cells washed three times with PBS, fixed in 2% PFA for 20 min at ambient temperature, permeabilized in 0.1% Triton X-100 for 15 min at ambient temperature. Cell nuclei were then counterstained using DAPI (300 nM; 5 min) after which the dishes were stored at 4°C until being viewed by epifluorescence microscopy (Nikon Cs1).

The number of QDot positive cells was determined by analyzing the microscopy images using ImageJ. From the collected images, more than 250 cells/condition out of 3 independent

experiments were analyzed for the total number of cell nuclei and the number of QDot-positive cells. Data are expressed as mean ± SEM and are gathered for more than 250 cells analyzed per condition. Data are given as the number of QDot positive cells over the total number of DAPI-stained cells.

2.4. Statistical analysis.

All data are expressed as mean ± SEM unless indicated otherwise and data were analyzed using one-way analysis of variance (ANOVA). When comparing different QDot concentrations to the same control group (the reference group), the Dunnett post-hoc analysis method was used. In all cases, the degree of significance is indicated when appropriate (* : $p < 0.05$; ** : $p < 0.01$; *** : $p < 0.001$).

3. Results and Discussion.

3.1. Nanoparticle characterization.

The synthesis of the PMA-QDots used in the present work has been well-documented in multiple studies. The PMA-QDots have been thoroughly characterized and display a decent batch-to-batch reproducibility [18, 28, 31]. The QDots used in the present study consist of spherical CdSe/ZnS core-shell structures with a diameter dc of the inorganic core-shell structure of around 4.7 ± 0.9 nm diameter, as assessed by transmission electron microscopy (**Supporting Figure S2**), with initially hydrophobic surfactant capping. These QDots are overcoated with PMA molecules, which are amphiphilic. The hydrophobic sidechains of PMA can interdigitate the hydrophobic surfactants on the original QDot surface, while the hydrophilic backbone renders the resulting QDots watersoluble [29]. Upon applying the PMA coating and transferring the QDots to an aqueous environment (10 mM phosphate buffered saline (PBS), pH 7.4), QDots with a

hydrodynamic diameter of d_h 11 $\pm$ 3 nm and a zeta potential of -18 $\pm$ 1 mV were obtained, as determined by dynamic light scattering (DLS) and electrophoretic mobility measurements, which is in line with previous reports. In PBS, the QDots remained stable in suspension for at least 3 months without any detectable agglomeration. The particles have a maximal emission at 597 nm and a quantum yield of 6.7%.

3.2. Cellular uptake of PMA-coated QDots.

In view of cell labeling and NP-toxicity studies, cell uptake levels and intracellular localization of the QDots must be carefully evaluated. Upon incubating the cells with 15 nM QDots, which is a typical QDot concentration used for cell labeling [18], confocal microscopy revealed endolysosomal localization of the QDots in all three cell types (**Figure 1A**) as is commonly observed for NPs [32-34]. For endosomal visualization, the lipophilic dye 3,3′-dioctadecyloxacarbocyanine perchlorate (DiO) was used. As this dye eventually will stain multiple intracellular compartments, the exposure time of the cells was kept low (30 min) in which case mostly endosomes will be stained positive. Additionally, the QDots themselves were only allowed to be taken up by the cells for 30 min, resulting in relatively low uptake values compared to data obtained after longer incubations (see, for instance, **Figure 4**). Note that due to the resolution limit of optical microscopy no individual QDots inside the endosomes can be resolved, and that the fluorescence signals originate from clusters of QDots within the same endosomal vesicles [35]. In order to obtain more quantitative information, the level of cell-associated Cd^{2+} was determined using a previously validated spectrophotometric technique [36], as described in the supporting information. In short, this fluorescent dye-based technique makes use of an increase in fluorescence that occurs when the dye binds free Cd^{2+} ions and has been used by multiple groups [32, 36]. Upon acidic digestion of cell-associated QDots, the level of

free Cd^{2+} is determined, from which the number of QDots is calculated using a dilution series of the QDot stock treated under identical conditions. The accuracy of this quantitative assessment therefore depends on the intrinsic problems associated with determining QDot concentrations and determining QDot-associated Cd^{2+} levels [16]. Therefore, the obtained absolute values are prone to error. However, relative values can be used for comparative purposes inbetween different experiments using the same samples. Quantitative determination of cellular QDot levels upon 24 h exposure to various QDot concentrations revealed a concentration-dependent, sub-linear increase in the number of QDots per cell as well as the total number of cell-associated QDots (**Figure 1B,C**), suggestive of a saturable endosomal uptake mechanism for the QDots. Interestingly, C17.2 and HUVEC cells had similar uptake levels, whereas PC12 cells had ingested lower numbers of QDots, which has been observed for various types of NPs [14, 37]. This is likely due to the smaller overall size of the PC12 cells and their smaller surface area, resulting in a reduced area of interaction of NPs with the cell membrane, hereby impeding NP uptake.

As the lipophilic dye DiO and the QDots could only be used for short exposure times, the intraendosomal localization of the QDots at later time points was further shown by transmission electron microscopy of the 3 different cell types, following a 24 h exposure to the QDots at 10 nM. This slightly lower concentration was selected to avoid conditions at which acute toxic effects occur, as this might lead to artifacts in terms of cell organelle structure and organization. **Figure 2** shows that for all three cell types, the QDots reside in vesicular structures, bearing the morphological features of endosomal or lysosomal compartments. Together, these data indicate that the particles are taken up through the endosomal pathway and finally reside in the

endolysosomal compartment, where they will be subjected to lower pH values, different ionic strengths and different protein compositions than in the extracellular or cytoplasmic environment.

3.3. Effect of pH-mediated QDot degradation on Cd^{2+} release and fluorescence intensity.

For cadmium-based QDots, one primary cause of toxicity has been suggested to be free Cd^{2+} ions [27, 28], a well-known metal toxicant [29, 38]. However, it also has been shown that a ZnS shell around the CdSe core slows down corrosion of the QDots and thus reduces cytotoxicity [28]. By using the fluorescent dye-based assay, the presence of free Cd^{2+} ions in the 2 μM QDot stock suspension was evaluated, showing levels of 3.9 μM of free Cd^{2+}. Comparison to the Cd^{2+} concentration after acidic digestion of the QDots, as determined with the same assay, demonstrates that in neutral aqueous solution approximately 1.6 % of the total Cd^{2+} content of the QDots is present as free Cd^{2+}, the rest is bound to the QDots. Please note that this percentage may depend on the QDot concentration. Under diluted conditions the equilibrium can shift towards a larger percentage of dissolved Cd^{2+}. In previous work we calculated the percentage of Cd^{2+} which is on the surface of the CdSe core to be around 4% (cf. the Supporting Information). Thus around 40% of the surface Cd^{2+} atoms from the CdSe cores (under the ZnS shell) in the 2 μM QDot stock solution had dissolved under equilibrium conditions.

Free Cd^{2+} has been found to be able to affect cells starting from concentrations of 1 μM, but this value has been found to be dependent of cell type and conditions of incubation [28]. In context with the determined value of 3.9 μM of free Cd^{2+} in the stock solution and the further dilution of the QDots in cell medium prior to cell labeling (at least by 100-fold) this suggests that the free QDot-derived Cd^{2+} (in the cell medium) is likely not to be solely responsible for acute cytotoxic effects. Although the dilution of the QDots will shift the equilibrium between free and NP-

associated Cd^{2+}, the high dilution levels used here will likely not shift the equilibrium to such extent that more than 1 µM of free Cd^{2+} could be obtained. This was further verified by exposing cells for 24 h to pre-conditioned medium that was previously exposed to the QDots at the concentrations used for cell labeling (up to 20 nM) for 24 h and was subsequently ultracentrifugated at 115584 g. This medium then only contained free ions derived from the diluted QDot stocks, which was found not to result in significant effects on cell viability (**Supporting Figure S5**).

Upon endosomal uptake, the QDots will however be exposed to varying environmental pH values, ranging from 7.4 for extracellular medium to 4.5 in the lysosomes. As acidic conditions are known to induce acid etching of the QDot surface and hereby release Cd^{2+} [37, 39], the effect of pH on Cd^{2+} release was evaluated using previously optimized endosomal-pH buffer systems [36] (see the Supporting Information for full experimental details). **Figure 1D** shows a clear pH-dependent release of Cd^{2+} under these cell-free conditions as a function of time, resulting in approximately a 15-fold increase in Cd^{2+} levels after 5 days at pH 4.5 compared to 5 days at pH 7.4.

The degradation of the QDots is also reflected in their fluorescence intensities, that rapidly drop upon exposure to lower pH values, but further decrease in time as a result of QDot surface etching (**Figure 3A**). Transferring the QDots to PBS at pH 7.4 restores the initial loss of fluorescence intensity back to near control levels, whereas for QDots that were exposed to acidic environments for several days, the fluorescence intensities could not be fully recovered (**Supporting Figure S4**). Additionally, the effect of the low pH has also been investigated using TEM, where micrographs were taken of QDots in organic phase (**Figure 3B1**) and of the same QDots after 2 days exposure to pH 3 (**Figure 3B2**). The data clearly indicate changes in the shape

of the QDots after exposure to low pH values, which is consistent with surface etching of the QDots and associated release of Cd^{2+} ions. To evaluate the extent and kinetics of intracellular QDot degradation, the level of intracellular Cd^{2+} was evaluated in non-proliferating cells, established as previously described (see Supporting Information for a full experimental methodology) [36]. Non-proliferating cells were used to enable an accurate follow-up of Cd^{2+} release in cells as a function of time, while minimizing the effect of QDot dilution due to cell division. The data show a clear time-dependent increase in cellular Cd^{2+} (only free Cd^{2+}, not QDot-associated Cd^{2+}) the level of which also correlated with intracellular QDot levels (**Figure 4**).

3.4. Effects of QDot degradation on cell viability.

Next, the cytotoxic effects of the QDots were evaluated, revealing a concentration-dependent toxicity in all three cell types, starting from 20 nM or higher for C17.2 and HUVEC cells and 30 nM for PC12 cells (**Figure 5A**). The latter is likely explained by the lower levels of cell-associated QDots for the PC12 cells (**Figure 1B**). Interestingly, when non-proliferating cells were loaded with QDots, the cytotoxic effects of the QDots significantly augmented in time, in close correlation with the elevated Cd^{2+} levels (**Supporting Figure S6**). When using $CdCl_2$ as a source of free Cd^{2+}, only minimal cytotoxic effects were observed. **Figure 6** shows the intracellular level of Cd^{2+} measured in C17.2 cells after 24 h exposure to $CdCl_2$ at various concentrations. The data reveal that at the highest dose (500 nM) $CdCl_2$), the intracellular level of Cd^{2+} was substantially higher than the level obtained when cells were exposed to QDots (**Figure 4C**). Therefore, the data collectively show that the toxicity induced by Cd^{2+} ions by $CdCl_2$ addition is less substantial than the toxicity induced by Cd^{2+} derived from intracellular QDot degradation. Caution must be considered when trying to explain the lack of effect of $CdCl_2$ at the “same intracellular

concentrations" as only free Cd^{2+} was considered and the Cd^{2+} still in the QDots, or the ions present on the QDot surface were not taken into account, which may all play a significant role in QDot-mediated toxicity. However, the low effects of free Cd^{2+} at high intracellular levels given by $CdCl_2$ suggest that other than immediate toxicity of free Cd^{2+}, different mechanisms appear to be contributing to the QDot-induced toxicity (**Supporting Figure S7, S8**). One possible explanation for the clear correlation between QDot-induced toxicity and intracellular QDot-derived Cd^{2+} levels, lies in the endosomal enclosure of the QDots [36]. Where Cd^{2+} derived from $CdCl_2$ can more freely distribute throughout the cell cytoplasm and will be taken up by the cell in a short time span, this is not the same for Cd^{2+} derived from cadmium-based QDots. The intraendosomal degradation of the QDots ~~may~~ likely result in a more heterogeneous distribution of Cd^{2+}, with very high local Cd^{2+} concentrations in a confined space (endosome) that easily exceed the toxic threshold, thereby affecting cell homeostasis. Additionally, the Cd^{2+} derived from QDots is gradually released over time and will immediately be subjected to a degradative environment of low pH, unlike the Cd^{2+} ions that are derived from $CdCl_2$. The presence of the ions in the low pH environment of the endosomes at high local concentrations may result in higher toxic effects than more homogeneously distributed Cd^{2+}. Furthermore, NPs such as QDots are known to affect cellular wellbeing, for instance by the induction of ROS. When cells are already subject to stress induced by the intracellular presence of NPs, the additional presence of Cd^{2+} will likely result in toxic effects more quickly than the same levels of Cd^{2+} would in cells that have no other stress inducers. This hypothesis also supports the earlier work of other groups [40, 41] who found that intracellular Cd^{2+} release was more toxic than extracellular Cd^{2+}.

These data collectively show that minor toxic effects occur at concentrations of 500 nM of free Cd^{2+}. Compared to the QDots, similar minor toxic effects were noticeable at concentrations of 10

nM. Whereas the amount of free intracellular Cd^{2+} derived from the QDots was much lower than Cd^{2+} levels derived from $CdCl_2$, the total amount of Cd^{2+} added was much higher in the case of the QDots (for 10 nM QDots; an experimental value of 1.32 μM Cd^{2+} was obtained). Based on these values, it can be concluded that the majority of QDot-associated Cd^{2+} is not released and remains confined within the QDot core. These ions do not appear to play any major role in the toxicological effects of Cd^{2+} as when comparing the toxicity of $CdCl_2$ and QDots based on the total amount of Cd^{2+} added, the QDots display less toxicity.

3.5. Effects of QDots on oxidative stress.

To further test this hypothesis, the effect of $CdCl_2$ and QDots on oxidative stress were evaluated in non-proliferating cells, indicating a clear concentration-dependent induction of reactive oxygen species (ROS) for either $CdCl_2$ or QDots (**Figure 5B, Supporting Figures S8, S9**). However, for the QDots, the level of ROS also increased in time, which is in line with the increasing Cd^{2+} concentrations. As the level of ROS is higher for the QDots than for $CdCl_2$, this supports our hypothesis on local high Cd^{2+} concentrations obtained upon intraendosomal QDot degradation. When cells were co-incubated with 5 mM N-acetylcystein (NAC), an FDA-approved free radical scavenger, ROS levels were reduced to near control levels (**Supporting Figure S8**). The addition of NAC was also able to partially restore cell viability (**Supporting Figure S6**), indicating that ROS are an important mediator in QDot-induced toxicity, but other mechanisms must also contribute to the overall cytotoxicity.

To evaluate whether the elevated ROS levels have any secondary effects on cell physiology, mitochondrial membrane potential (ΔΨm) and DNA damage were evaluated. The ΔΨm was

evaluated using the JC-10 dye, which remains in the cytoplasm as green monomers until it is taken up by healthy mitochondria with a normal ΔΨm, which will make the dye aggregate and its fluorescence emission will shift (red colour). The ratio of green over red (as shown in **Figure 5C**) therefore indicates the ratio of damaged over healthy mitochondria. The data show that, in line with the onset of ROS, at QDot concentrations from 10 nM and above, a clear and significant increase in damaged mitochondria can be seen, at levels below those at which acute toxicity occurs (30 nM). The significant effects at concentrations below toxic levels clearly indicate that these results are not artifacts caused by cell death, but rather that the QDot-mediated onset of ROS precedes cell death. Together with the observation that NAC treatment can partially overcome QDot-induced toxicity, these results show that ROS induction is one of the prime mechanisms by which these NPs elicit toxic effects.

As elevated ROS levels are known to possibly result in DNA damage, which may have far-reaching consequences in the safety of these materials as this a hallmark of carcinogenicity, the occurrence of DNA double strand breaks was evaluated (**Figure 5C**). This was done by staining for phosphorylated γ-H2Ax foci, that are formed by the rapid phosphorylation of histone H2Ax at sites of DNA double strand breaks. Similar as for the loss of ΔΨm, significant DNA damage was found to occur at doses at which acute toxicity was minimal (20 nM).

Taken together, these data indicate that the QDot-induced ROS levels result in secondary effects which, at higher levels will result in cell death, but are still significant even at lower levels, where they induce cell stress or carcinogenicity.

3.6. Effects of QDots on cell morphology and functionality.

To further refine the non-toxic concentration of PMA-coated QDots and to analyze the contribution of time-dependent Cd^{2+} release, the morphology of QDot-exposed HUVECs was evaluated. As a primary human cell type with a typical well-spread morphology, these cells are perfectly suited to assess QDot-mediated disturbance of actin or tubulin cytoskeleton [14]. Furthermore, previous data on iron oxide NPs have shown that cell deformations usually occur after 2-3 days after initial cell exposure [14], making this an interesting parameter to study with respect to time-dependent Cd^{2+} release. **Figure 7A,B** reveals a concentration-dependent reduction in cell-spreading, which is in line with previous reports on various types of nanoparticles [36, 42, 43]. Please note that for these assays, only low QDot concentrations (up to 20 nM) were selected that do not induce significant levels of acute cell death as the occurrence of apoptotic bodies or condensed cells would substantially influence the results obtained. The reduction in cell spreading correlates well with the onset of ROS, suggesting a possible influence of ROS in the cytoskeletal deformations. However, previous data have suggested the conjoined effects of multiple mechanisms to play a role in cell deformations, including 1) the endosomal localization of QDots resulting in enlarged lysosomal compartments [30] and 2) a loss of lysosomal functionality, resulting in large compartments containing high numbers of rigid NPs and hereby occupying a substantial part of the cellular cytoplasmic compartment, sterically hindering normal cytoplasmic functionality [36].

Next, the effect of the QDots on cell functionality was investigated. To evaluate the effect of Cd^{2+} release, the PC12 model system was used, which was previously found to be an excellent model for a fast, sensitive and quantifiable assessment of cell functionality upon nanoparticle exposure. In this assay, cell functionality is evaluated by induction of neurite outgrowth upon stimulation with nerve growth factor (NGF) [13]. When cells were exposed to QDots at

nominally non-toxic concentrations, the outgrowth of neurites after 2 days of stimulus with NGF (4 days after initial cell exposure) was found to be significantly impeded at higher QDot concentrations (**Figure 7C,D**).

3.7. Assessment of QDot functionality for comparative data analysis.

Based on all the data obtained, the non-cytotoxic concentration of PMA-coated core/shell QDots of 4.7 nm CdSe/ZnS diameter is around 2 nM. Previously, the multiparametric methodology applied in the current study has been used to evaluate PMA-coated Au NPs of the same size and identical (PMA) surface coating [43] as well as commercially available polymer-coated core/shell QDots [36]. For the Au particles, the non-toxic level was found to be 10 nM, indicating a 5-fold higher toxicity of the QDots, owing to differences in the metal core of the NPs and the forthcoming photophysical properties of these materials as QDots, for instance, are well-known to produce ROS under light irradiation which less outspoken for Au NPs. Interestingly this value fits remarkably to very early studies, in which PMA-coated CdSe/ZnS QDots were found to be more than 3 times toxic than PMA-coated Au NPs [28]. Given the difficulties in accurately assessing NP concentrations [16], differences in the uniformity by which the PMA polymer covers the NPs and polydispersity differences between the two different NP types, these absolute values should however be treated with care and making comparisons should be done cautiously.

Given the difficulties in comparing different NPs due to the problems associated with accurately determining NP concentrations [16], the applicability of the QDots for fluorescence cell tracking was evaluated at their non-toxic concentration (2 nM). In previous work, it was found that carboxyl-functionalized commercially available QDots of similar size tested under identical conditions were found to be non-toxic at 1 nM [36]. Note that also the PMA-coated QDots as

used in this study are terminated by carboxyl-groups. Differences in the methods used for determining QDot concentrations are most likely the reason for the slight difference in the values of these studies [16]. At non-toxic concentrations, labeled cells were able to be monitored by fluorescence microscopy for approximately 4 cell doublings (**Figure 8**). In the end, the duration by which QDot labeled cells could be efficiently visualized at non-toxic conditions (approximately 4 cell doublings) was the same for both types of carboxylated Qdots (commercial and synthesized ones), indicating that both types of QDots resulted in similar efficiencies in terms of cell labeling strategies. The ability to track the cells by fluorescence microscopy is influenced by the number of QDots internalized by the cell, as well as other factors such as their coating, quantum yield. These data demonstrate that when assessing NP toxicity, the number of cell-associated NPs determines cytotoxic effects rather than the total number of NPs added to the cells, which is in line with earlier findings [44]. Here, we demonstrated the importance of intracellular NP concentrations in the cytotoxicity of nanomaterials as well as the necessity to assess the functionality of the nanomaterials at non-toxic conditions. In the end, it is important to evaluate whether the NPs at their non-toxic concentration are still functional for the desired application, such as cell tracking. Especially given the difficulties in accurately determining NP concentrations, assessing their biomedical functionality appears like an informative and fruitful tool, which allows to compare particles with respect to both toxicological and technical features of the NPs, thereby providing a good overview of the respective NP strength for a selected purpose.

4. Conclusions.

In conclusion, the present work demonstrates the importance of NP degradation in the cellular microenvironment in the cytotoxic effects of nanomaterials. Therefore, the data collectively show

that the toxicity induced by Cd^{2+} ions by $CdCl_2$ addition is less substantial than the toxicity induced by Cd^{2+} derived from intracellular QDot degradation (when compared at the same intracellular free Cd^{2+} concentration). Please note that under the conditions used in this study, the majority of QDot-associated Cd^{2+} is not released and remains confined within the QDot core. These ions do not appear to play any major role in the toxicological effects of Cd^{2+} as when comparing the toxicity of $CdCl_2$ and QDots based on the total amount of Cd^{2+} added, the QDots display less toxicity. Together, these data reveal that while current cadmium-containing QDots are well-suited for monitoring cell behavior by fluorescence microscopy for a low number of cell divisions, Cd^{2+}-based QDot formulations do not appear to be optimally suited for long-term cell tracking after endosomal uptake. Optimization of QDot formulations can occur at both the level of the QDot core as at the level of the coating applied for QDot biofunctionalization. The current study demonstrates the need for specialized model systems, such as non-proliferating cells in order to be able to study this effect in more detail at later time points under conditions close to relevant physiological conditions. Additionally, there is a need for techniques that enable to determine the chemical state of all NP-associated ions in real-time in live cells. Considering the technical difficulties in terms of accurately assessing NP concentrations, it is also vital to accurately assess functional (= cell-associated) NP levels. In order to enable a comparison of different NPs, it is therefore more suited to use NP functionality (e.g. the ability to fluorescently visualize labeled cells) at non-toxic concentrations as the final parameter which determines NP safety, rather than comparing various NP concentrations, which may not be very insightful.

5. Acknowledgements.

SJS is a postdoctoral fellow from the FWO-Vlaanderen. Financial support from the FWO-Vlaanderen (Krediet aan Navorsers to SJS), the UGent consortium NB Photonics, and from the

European commission (grant Nandiatream to WJP) are gratefully acknowledged. The authors wish to thank Prof. Alain R. Brisson, Université Bordeaux, for their expertise in cellular TEM.

6. References.

1. Magnuson BA, Jonaitis TS, Card JW. A brief review of the occurrence, use, and safety of food-related nanomaterials. J Food Sci 2011;76:R126-33.

2. Nasir A, Friedman A. Nanotechnology and the Nanodermatology Society. J Drugs Dermatol 2010;9:879-82.

3. Report L. Nanomaterials state of the market: Stealth success, broad impact. Available from: http://portalluxresearchinecom/research/document3735:2008 2008.

4. Fairbrother A, Fairbrother JR. Are environmental regulations keeping up with innovation? A case study of the nanotechnology industry. Ecotox Environment Safety 2009;72:1327-30.

5. Faunce T, Watal A. Nanosilver and global public health: international regulatory issues. Nanomedicine (Lond) 2010;5:617-32.

6. Hamburg MA. Science and regulation. FDA's approach to regulation of products of nanotechnology. Science 2012;336:299-300.

7. Soenen SJ, Demeester J, De Smedt SC, Braeckmans K. Turning a frown upside down: Exploiting nanoparticle toxicity for anticancer therapy. Nano Today 2013;8:121-125.

8. Chen Y, Qu K, Zhao C, Wu L, Ren J, Wang J, Qu X. Insights into the biomedical effects of carboxylated single-wall carbon nanotubes on telomerase and telomeres. Nature Comm. 2012;3:1074.

9. Joris F, Manshian BB, Peynshaert K, De Smedt SC, Braeckmans K, Soenen SJ. Assessing nanoparticle toxicity in cell-based assays: influence of cell culture parameters and optimized models for bridging the in vitro-in vivo gap. Chem Soc Rev 2013;DOI: 10.1039/C3CS60145E.

10. Thomas CR, Xia T, Rallo R, Zhao Y, Ji Z, Lin S, et al. Nanomaterials in the environment: from materials to high-throughput screening to organisms. ACS Nano 2011;5:13-20.

11. Soenen SJ, Rivera-Gil P, Montenegro JM, Parak WJ, De Smedt SC, Braeckmans K. Cellular toxicity of inorganic nanoparticles: Common aspects and guidelines for improved nanotoxicity evaluation. Nano Today 2011;6:446-65.

12. Elder A, Yang H, Gwiazda R, Teng X, Thurston S, He H, et al. Testing nanomaterials of unknown toxicity: An example based on platinum nanoparticles of different shapes. Advanced Mater 2007;19:3124-8.

13. Pisanic TR, 2nd, Blackwell JD, Shubayev VI, Finones RR, Jin S. Nanotoxicity of iron oxide nanoparticle internalization in growing neurons. Biomaterials 2007;28:2572-81.

14. Soenen SJ, Himmelreich U, Nuytten N, De Cuyper M. Cytotoxic effects of iron oxide nanoparticles and implications for safety in cell labelling. Biomaterials 2011;32:195-205.

15. Rivera Gil P, Oberdorster G, Elder A, Puntes V, Parak WJ. Correlating physico-chemical with toxicological properties of nanoparticles: the present and the future. ACS Nano 2010;4:5527-31.

16. Rivera-Gil P, Jimenez De Aberasturi D, Wulf V, Pelaz B, Del Pino P, Zhao Y, et al. The challenge to relate the physicochemical properties of colloidal nanoparticles to their cytotoxicity. Acc Chem Res 2013;46:743-9.

17. Chan WCW, Maxwell DJ, Gao XH, Bailey RE, Han MY, Nie SM. Luminescent quantum dots for multiplexed biological detection and imaging. Curr Opin Biotech 2002;13:40-6.

18. Rivera-Gil P, Yang F, Thomas H, Li L, Terfort A, Parak WJ. Development of an assay based on cell counting with quantum dot labels for comparing cell adhesion within cocultures. Nano Today 2011;6:20-7.

19. Azzazy HM, Mansour MM, Kazmierczak SC. From diagnostics to therapy: prospects of quantum dots. Clin Biochem 2007;40:917-27.

20. Bhirde A, Xie J, Swierczewska M, Chen X. Nanoparticles for cell labeling. Nanoscale 2011;3:142-53.

21. Wu X, Liu H, Liu J, Haley KN, Treadway JA, Larson JP, et al. Immunofluorescent labeling of cancer marker Her2 and other cellular targets with semiconductor quantum dots. Nat Biotechnol 2003;21:41-6.

22. Pinaud F, Clarke S, Sittner A, Dahan M. Probing cellular events, one quantum dot at a time. Nat Methods 2010;7:275-85.

23. Kim S, Lim YT, Soltesz EG, De Grand AM, Lee J, Nakayama A, et al. Near-infrared fluorescent type II quantum dots for sentinel lymph node mapping. Nat Biotechnol 2004;22:93-7.

24. Ballou B, Ernst LA, Andreko S, Harper T, Fitzpatrick JAJ, Waggoner AS, et al. Sentinel lymph node imaging using quantum dots in mouse tumor models. Bioconj Chem 2007;18:389-96.

25. Tsay JM, Trzoss M, Shi LX, Kong XX, Selke M, Jung ME, et al. Singlet oxygen production by peptide-coated quantum dot-photosensitizer conjugates. J Am Chem Soc 2007;129:6865-71.

26. Zhu XC, Lu WT, Zhang YZ, Reed A, Newton B, Fan Z, et al. Imidazole-modified porphyrin as a pH-responsive sensitizer for cancer photodynamic therapy. Chem Commun 2011;47:10311-3.

27. Derfus AM, Chan WCW, Bhatia SN. Probing the cytotoxicity of semiconductor quantum dots. Nano Lett 2004;4:11-8.

28. Kirchner C, Liedl T, Kudera S, Pellegrino T, Javier AM, Gaub HE, et al. Cytotoxicity of colloidal CdSe and CdSe/ZnS nanoparticles. Nano Lett 2005;5:331-8.

29. Chen N, He Y, Su Y, Li X, Huang Q, Wang H, et al. The cytotoxicity of cadmium-based quantum dots. Biomaterials 2012;33:1238-44.

30. Ambrosone A, Mattera L, Marchesano V, Quarta A, Susha AS, Tino A, et al. Mechanisms underlying toxicity induced by CdTe quantum dots determined in an invertebrate model organism. Biomaterials 2012;33:1991-2000.

31. Zhang F, Lees E, Amin F, Gil PR, Yang F, Mulvaney P, et al. Polymer-coated nanoparticles: A universal tool for biolabelling experiments. Small 2011;7:3113-27.

32. Cho SJ, Maysinger D, Jain M, Roder B, Hackbarth S, Winnik FM. Long-term exposure to CdTe quantum dots causes functional impairments in live cells. Langmuir 2007;23:1974-80.

33. Soenen SJ, Brisson AR, Jonckheere E, Nuytten N, Tan S, Himmelreich U, et al. The labeling of cationic iron oxide nanoparticle-resistant hepatocellular carcinoma cells using targeted magnetoliposomes. Biomaterials 2011;32:1748-58.

34. Parak WJ, Boudreau R, Le Gros M, Gerion D, Zanchet D, Micheel CM, et al. Cell motility and metastatic potential studies based on quantum dot imaging of phagokinetic tracks. Advanced Mater 2002;14:882-5.

35. Brandenberger C, Muhlfeld C, Ali Z, Lenz AG, Schmid O, Parak WJ, et al. Quantitative evaluation of cellular uptake and trafficking of plain and polyethylene glycol-coated gold nanoparticles. Small 2010;6:1669-78.

36. Soenen SJ, Demeester J, De Smedt SC, Braeckmans K. The cytotoxic effects of polymer-coated quantum dots and restrictions for live cell applications. Biomaterials 2012;33:4882-8.

37. Moulis JM. Cellular mechanisms of cadmium toxicity related to the homeostasis of essential metals. Biometals 2010;23:877-96.

38. Su Y, Hu M, Fan C, He Y, Li Q, Li W, et al. The cytotoxicity of CdTe quantum dots and the relative contributions from released cadmium ions and nanoparticle properties. Biomaterials 2010;31:4829-34.

39. Soenen SJ, Himmelreich U, Nuytten N, Pisanic TR, 2nd, Ferrari A, De Cuyper M. Intracellular nanoparticle coating stability determines nanoparticle diagnostics efficacy and cell functionality. Small 2010;6:2136-45.

40. Chang E, Thekkek N, Yu WW, Colvin VL, Drezek R. Evaluation of quantum dot cytotoxicity based on intracellular uptake. Small 2006;2:1412-7.

41. Schneider R, Wolpert C, Guilloteau H, Balan L, Lambert J, Merlin C. The exposure of bacteria to CdTe-core quantum dots: the importance of surface chemistry on cytotoxicity. Nanotechnol 2009;20:225101.

42. Mahto SK, Park C, Yoon TH, Rhee SW. Assessment of cytocompatibility of surface-modified CdSe/ZnSe quantum dots for BALB/3T3 fibroblast cells. Toxicol in Vitro 2010;24:1070-7.

43. Soenen SJ, Manshian B, Montenegro JM, Amin F, Meermann B, Thiron T, et al. The cytotoxic effects of gold nanoparticles: A multiparametric study. ACS Nano 2012;6:5767-83.

44. Soenen SJ, Manshian B, Doak SH, De Smedt SC, Braeckmans K. Fluorescent non-porous silica nanoparticles for long-term cell monitoring: Cytotoxicity and particle functionality. Acta Biomaterialia 2013; DOI: 10.1016/j.actbio.2013.04.026

Figure legends.

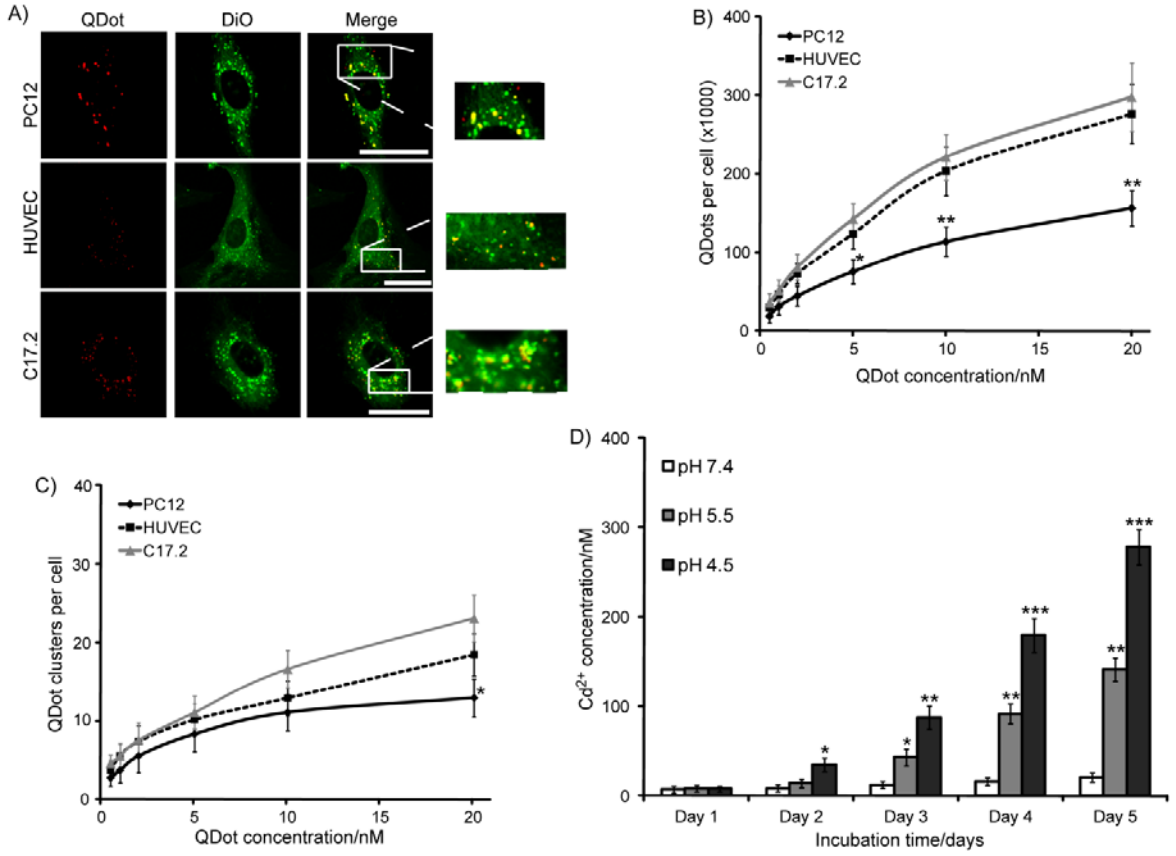

Figure 1: A) Representative confocal images of PC12 (top row), HUVEC (middle row) and C17.2 cells (bottom row) incubated with 15 nM PMA-coated QDots (left column: red) for 30 min in the presence of the lipophilic dye DiO (middle column: green). A merged image of both the QDots and the DiO positive endosomes is shown in the right column where the percentage of colocalization of both QDots and DiO positive endosomes is shown in the top right corner. Scale bars: 30 µm. B) The total number of QDots per cell as a function of the QDot concentration after 24 h incubation. C) The number of QDot containing endosomal vesicles per cell as quantified from the microscopy images after 24 h of cell exposure to the QDots. Data are shown as mean ± SEM (n = 4). For B and C, any difference between the different cell types in terms of total QDots

per cell or total QDot clusters per cellvis indicated when statistically significant (*: $p < 0.05$; **: $p < 0.01$; ***: $p < 0.001$). D) Levels of free Cd^{2+} in suspensions of PMA-coated QDots at various pH values (7.4, 5.5, 4.5) as a function of time as determined by acid digestion of the QDots followed by quantitation of the level of Cd^{2+} by means of Cd^{2+}-responsive fluorescence dye as described in the Supporting Information. Data are expressed as mean $\pm$ SEM (n = 3). When appropriate, the degree of significance for any condition compared to the control value at pH 7.4 is indicated (*: $p < 0.05$; **: $p < 0.01$; ***: $p < 0.001$).

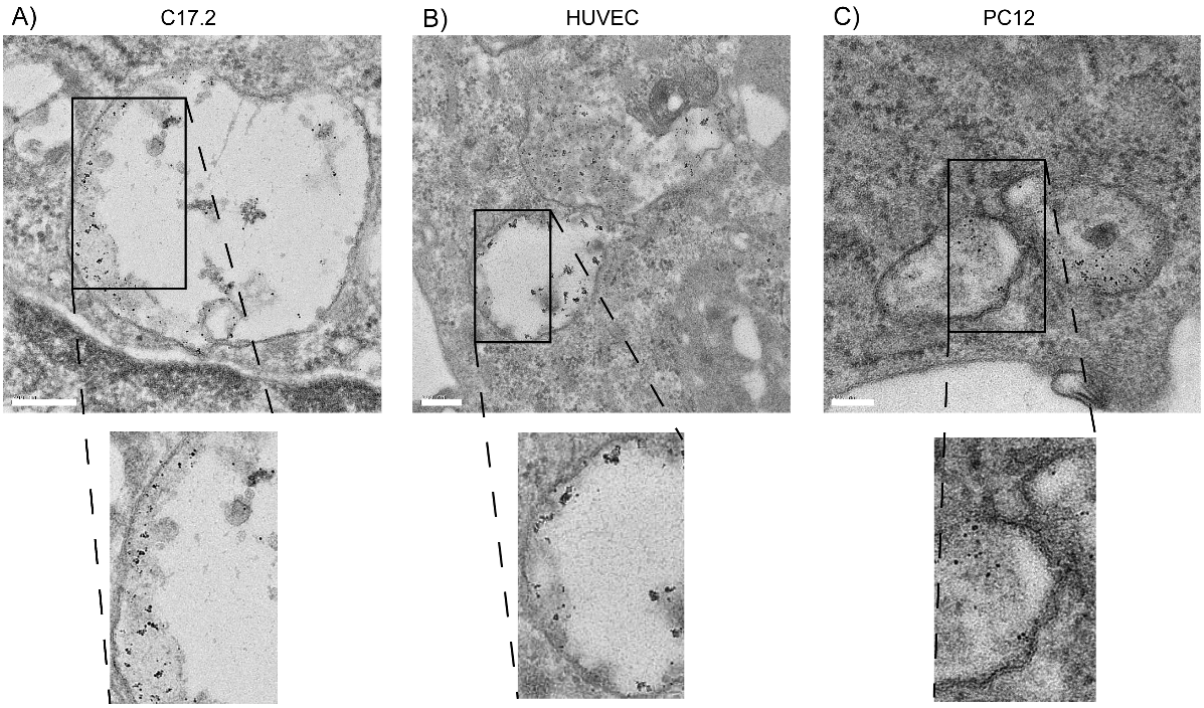

Figure 2: Transmission electron micrographs of A) C17.2, B) HUVEC and C) PC12 cells exposed to QDots for 24 h at 10 nM. The bottom figures are enlarged views of the respective areas indicated in the top figures. Scale bars: A, B: 200 nm, C: 100 nm.

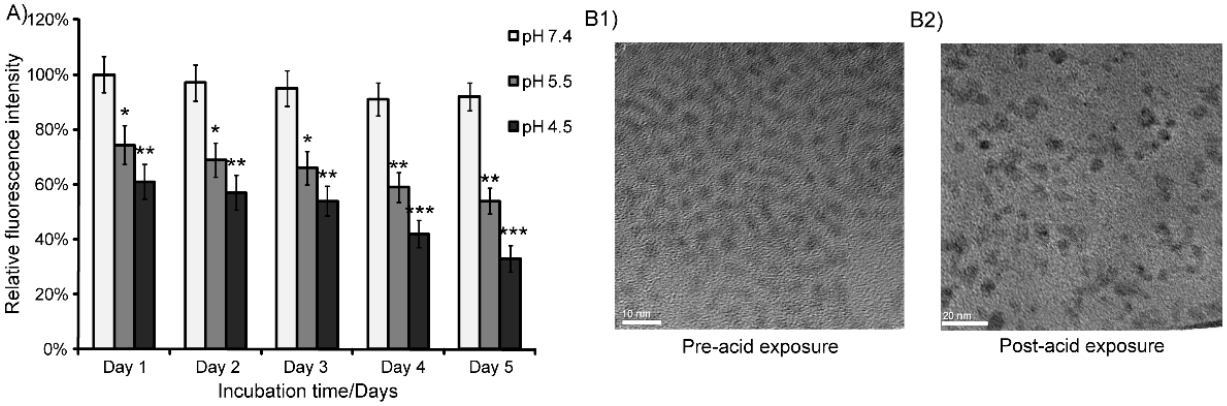

Figure 3: A) Effect of pH on QDot fluorescence intensity. Relative fluorescence intensity levels of 5 nM suspensions of PMA-coated QDots at various pH values (7.4, 5.5, 4.5) as a function of time. Data are expressed as mean $\pm$ SEM (n = 3) and the degree of statistical significance of treated samples versus control samples is indicated when appropriate (*: $p < 0.05$; **: $p < 0.01$; ***: $p < 0.001$). B) Transmission electron micrographs of the QDots upon synthesis (B1) and after 2 days exposure to pH 3 (B2). Scale bars: B1: 10 nm, B2: 20 nm.

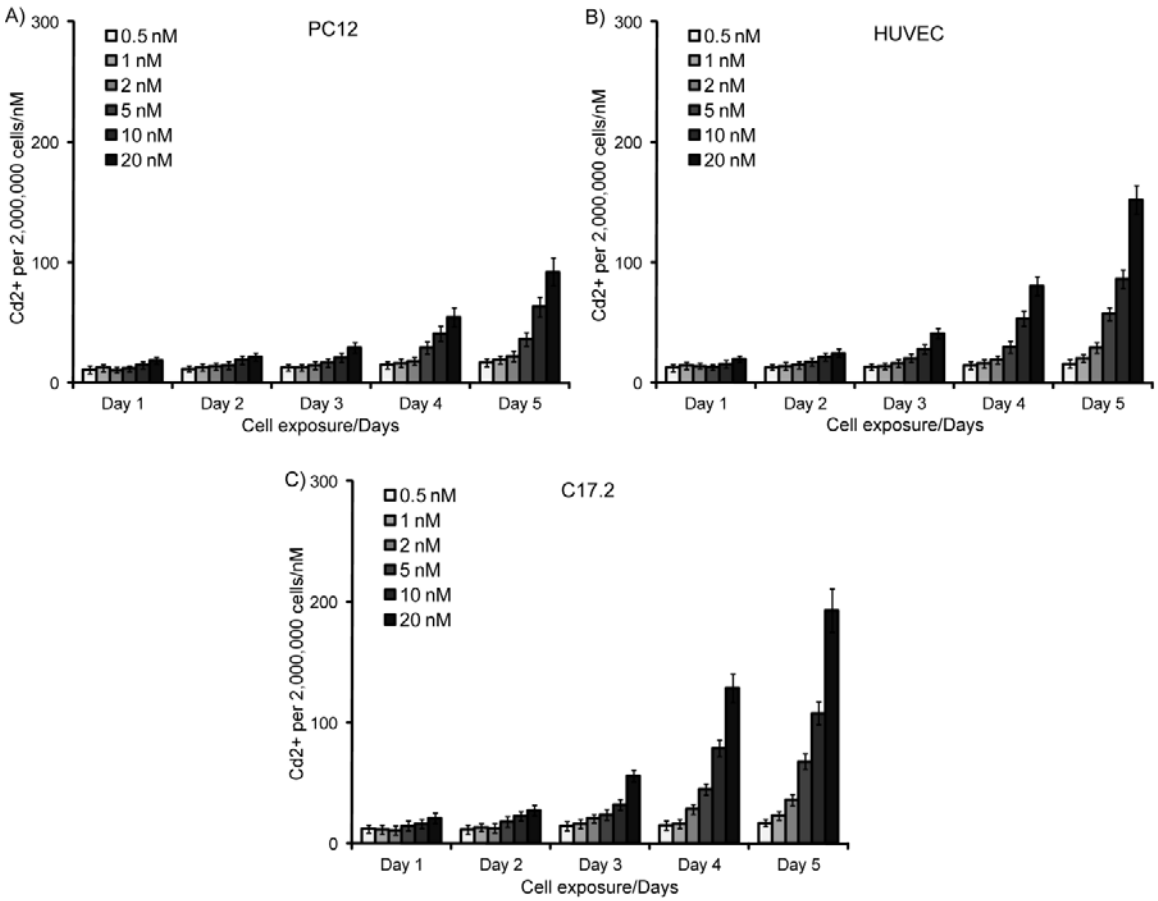

Figure 4: A-C) Levels of free Cd^{2+} in A) PC12, B) HUVEC and C) C17.2 cells exposed to various concentrations of PMA-coated QDots for 24 h and subsequently kept in non-proliferating state after which the cellular Cd^{2+} levels are measured after 1, 2, 3, 4 and 5 days. Data are expressed as mean $\pm$ SEM (n = 3). Please note that only free Cd^{2+} was measured, no acid digestion was employed and any remaining QDots were found not to significantly interfere with the assay readout.

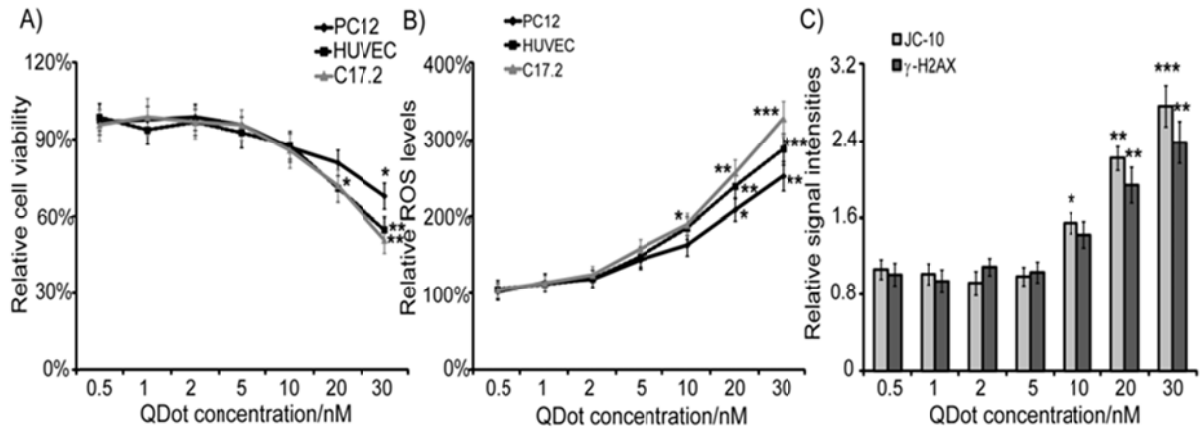

Figure 5: A) Viability and B) ROS induction of PC12, HUVEC and C17.2 cells as a function of QDot concentration after 24 h incubation. Data are represented as mean ± SEM (*n* = 6) and expressed as relative to untreated control cells. C) Quantitative levels of JC-10 (light grey) and γ-H_2Ax (dark grey) for HUVEC cells exposed for 24 h to different concentrations of QDots. Data are expressed as mean ± SEM (n = 3) and are presented as relative to that of untreated control cells (= 100%). When appropriate, the degree of significance is indicated (*: $p < 0.05$; **: $p < 0.01$; ***: $p < 0.001$).

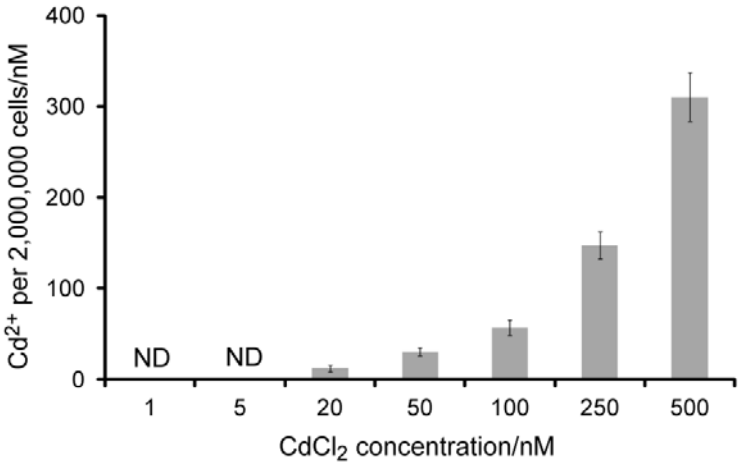

Figure 6: Levels of free Cd^{2+} in C17.2 cells exposed to various concentrations (1, 5, 20, 50, 100, 250 and 500 nM) of $CdCl_2$ for 24 h. Data are expressed as mean $\pm$ SEM (n = 3). ND: Non-detectable (values are within noise-level of the assay and cannot be distinguished from the background level).

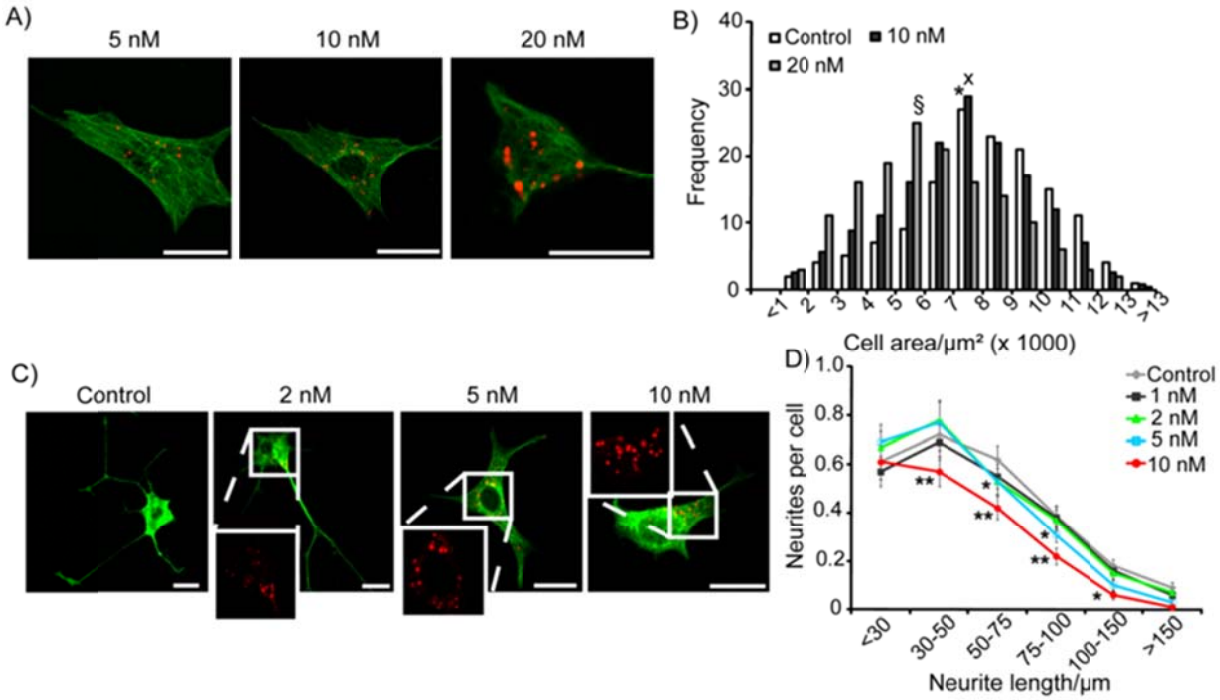

Figure 7: A) Representative confocal images of HUVEC cells exposed for 24 h to PMA-coated QDots at 5 nM (left column), 10 nM (middle row) and 20 nM (right column). The images shown are merged images of QDots (red) and α-tubulin cytoskeleton (green). Scale bars: 50 µm. B) Histograms representing the cell area distribution of HUVECs exposed to PMA-coated QDots for 24 h and stained after 2 additional days of culture. The average cell areas are indicated with * for control cells, X for 10 nM-treated cells and § for 20 nM-treated cells. C) Effect of QDots on PC12 cell functionality. Representative confocal images of PC12 cells exposed to PMA-coated QDots for 24 h at 0 (left column), 2 (2nd column), 5 (3rd column) or 10 nM (4th column) and subsequently exposed to nerve growth factor (NGF; 100 ng/ml) for 2 days. Images shown are merged images of QDots (red) and α-tubulin (green). The area indicated by the white rectangle is magnified at the bottom of the image, showing only the QDot fluorescence. Scale bars: 30 µm. (D) The number of neurites of a certain length per cell after 3 days of NGF exposure for cells exposed to 0, 1, 2, 5 or 10 nM of PMA-coated QDots. When appropriate, the degree of

significance is given when compared with untreated control cells (*: $p < 0.05$; **: $p < 0.01$; ***: $p < 0.001$).

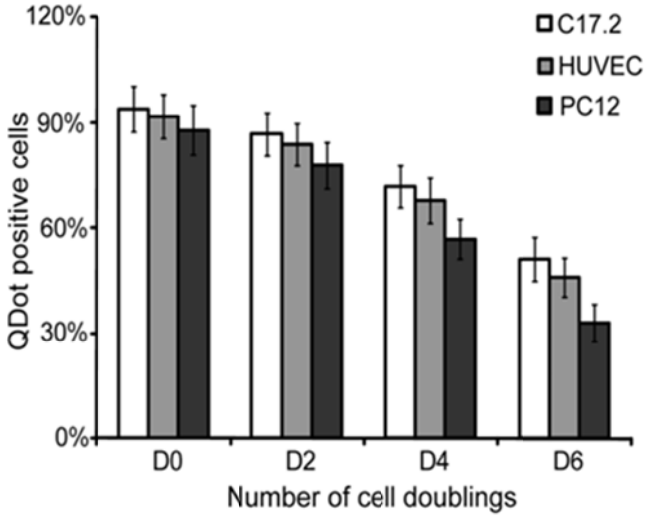

Figure 8: The percentage of QDot positive cells for cells incubated with 2 nM QDots for 24 h after 0, 2, 4 and 6 average cell doubling times as evaluated by microscopy analysis. The data are expressed as mean $\pm$ SEM ($n = 3$).